

Equations of state, transport properties, and compositions of argon plasma: Combination of self-consistent fluid variation theory and linear response theory

W. L. Quan,^{1,2} Q. F. Chen,^{1,*} Z. J. Fu,¹ X. W. Sun,² J. Zheng,¹ and Y. J. Gu¹

¹National key Laboratory of Shock Wave and Detonation Physics, Institute of Fluid Physics, CAEP, Mianyang 621900, China

²School of Mathematics and Physics, Lanzhou Jiaotong University, Lanzhou 730070, China

(Received 14 October 2014; revised manuscript received 13 January 2015; published 24 February 2015)

A consistent theoretical model that can be applied in a wide range of densities and temperatures is necessary for understanding the variation of a material's properties during compression and heating. Taking argon as an example, we show that the combination of self-consistent fluid variational theory and linear response theory is a promising route for studying warm dense matter. Following this route, the compositions, equations of state, and transport properties of argon plasma are calculated in a wide range of densities (0.001–20 g/cm³) and temperatures (5–100 kK). The obtained equations of state and electrical conductivities are found in good agreement with available experimental data. The plasma phase transition of argon is observed at temperatures below 30 kK and density about 2–6 g/cm³. The minimum density for the metallization of argon is found to be about 5.8 g/cm³, occurring at 30–40 kK. The effects of many-particle correlations and dynamic screening on the electrical conductivity are also discussed through the effective potentials.

DOI: [10.1103/PhysRevE.91.023106](https://doi.org/10.1103/PhysRevE.91.023106)

PACS number(s): 52.25.Jm, 52.25.Fi, 52.27.Gr

I. INTRODUCTION

Under compression, matter will go into the so-called warm dense matter (WDM) state characterized by strong coupling, partial degeneration, and partial ionization. Generally, the density of WDM is 0.01–10 times the solid density and the temperature varies in a range of 0.1–100 eV [1]. The knowledge of WDM is of fundamental importance—not only because of its appearance in inertial confined fusion [2] and in many celestial bodies such as Jupiter [3] and Neptune [4], which is relevant to the understanding of thermonuclear, laser, and other pulsed devices that require considerable energy density—but also because it reaches the boundary of our theories of matter: it is too dense for traditional plasma physics and too hot for traditional condensed matter physics [1].

Various methods of many-body theory have been developed to calculate the thermodynamics and transport properties of WDM. For examples, path integral Monte Carlo (PIMC) simulations were carried out for warm dense hydrogen [5] helium [6], a mixture of hydrogen and helium [7], water, and carbon [8]. Quantum molecular dynamics (QMD) simulations based on finite-temperature density functional theory (FTDFT) were also performed for warm dense hydrogen [9], helium [10], beryllium [11], aluminum [12], water [13], and iron [14], etc. Besides these *ab initio* calculations, several methods, such as the self-consistent averaged-atom model [15,16], classical and quantum hypernetted chain [17,18], activity expansion [19], and a self-consistent fluid variational theory [10,20–32], have also been widely used to study the warm dense matter. Even so, the understanding of this exotic state is still poor because of its inherent complexity. Up to now, the PIMC simulations, the strictest among these methods, have only been carried out for few-electron systems such as hydrogen and helium; it is still formidable for a substance like argon that has many electrons, while the results of QMD based on FTDFT are also not so satisfied at high temperature due to the

approximations that have to be used in FTDFT. For example, hydrogen and deuterium have been simulated with QMD by many groups, but the predicted Hugoniot are inconsistent with each other, especially at high temperature and density; see Fig. 5 in Ref. [33].

In our previous works [29–32], a self-consistent fluid variational theory (SFVT) was developed to calculate the equations of state (EOS) of hydrogen, deuterium, nitrogen, oxygen, and noble gases. In this paper, the SFVT is extended to be applicable in a wide range of density and temperature. The compositions and the EOSs of argon plasma are calculated for temperature up to 100 kK and density up to 20 g/cm³. Based on the compositions given by SFVT, the transport properties, including electrical conductivity, thermal conductivity, and thermopower, are further calculated with linear response theory (LRT) [34–40]. The aim of this paper is to illustrate the powerful predictive capability of the combination of SFVT and LRT in WDM research.

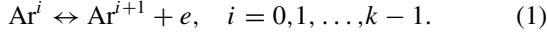
We select argon as representative since (1) argon plasma, as one of noble gases, is relatively simple because of the absence of molecule and the spherical symmetry of its atom. (2) The ideal potential energy for ionizing an isolate argon atom ($\text{Ar} \rightarrow \text{Ar}^+ + e$) is 15.76 eV, which is moderate, and thus a continuous transition is expected from a state with a small degree of ionization to a fully ionized state as the temperature and density increase. (3) Many theoretical methods used for hydrogen and helium have not been extended to argon. For example, the QMD simulation of warm dense argon has not been reported so far.

We organize this paper as follows. The self-consistent fluid variational theory to derive the compositions and the EOSs of argon plasma is presented in Sec. II. The linear response theory for transport properties is briefly outlined in Sec. III. The obtained results, including compositions, equations of state, transport properties, and the influence of many-particle correlations and dynamic screening are discussed in Sec. IV compared with experiments and other calculations, followed by a conclusion in Sec. V.

*Corresponding author: chenqf01@gmail.com

II. SELF-CONSISTENT FLUID VARIATIONAL THEORY

At sufficient high temperature and density, argon atom could be ionized into ion and electrons. Within the chemical picture, we suppose the system consisting Ar, Ar⁺, . . . , Ar^{k+} and electrons. k denotes the highest charge state achieved in the system. The compositions of such multicomponent plasma are governed by the reactions



When the local equilibrium of reaction is reached, the following condition should be satisfied:

$$\mu_i + I_i^{\text{eff}} = \mu_{i+1} + \mu_e, \quad i = 0, 1, \dots, k-1, \quad (2)$$

where I_i^{eff} denotes the effective ionization potential. μ_i and μ_e are the chemical potential of Arⁱ⁺ and electron, defined by

$$\mu_i = \left[\frac{\partial F^{\text{tot}}(T, V, N_0, N_1, \dots, N_k, N_e)}{\partial N_i} \right]_{T, V, N_{j \neq i}}, \quad (3)$$

$$i = 0, 1, \dots, k, e,$$

where F^{tot} , depending on $\{T, V, N_0, N_1, \dots, N_k, N_e\}$, is the total Helmholtz free energy of the system. T and V are the temperature and specific volume. N_i and N_e are the number of Arⁱ⁺ and electrons in this specific volume.

For ideal plasma where the interactions between particles are completely neglected, the effective ionization potential is just the ideal one, i.e., the energy necessary for ionizing an isolate atom (or ionizing an isolate ion further). However, as density increases, the interactions between particles become important and result in the lowering of ionization potential (LIP), reflecting the pressure induced ionization. To evaluate the effective ionization potential or the LIP arising from the interactions, the total Helmholtz free energy is divided into an ideal part and a correction part:

$$F^{\text{tot}} = F^{\text{id}} + F^{\text{cor}}. \quad (4)$$

Correspondingly, the definition of chemical potential, Eq. (3), is extended as

$$\mu_i^{\text{id}} = \left(\frac{\partial F^{\text{id}}}{\partial N_i} \right)_{T, V, N_{j \neq i}}, \quad \Delta \mu_i = \left(\frac{\partial F^{\text{cor}}}{\partial N_i} \right)_{T, V, N_{j \neq i}}, \quad (5)$$

$$i = 0, 1, \dots, k, e,$$

and the condition for the chemical equilibrium, Eq. (2), is rewritten as

$$\mu_i^{\text{id}} + \Delta \mu_i + I_i^{\text{id}} + \Delta I_i = \mu_{i+1}^{\text{id}} + \Delta \mu_{i+1} + \mu_e^{\text{id}} + \Delta \mu_e, \quad (6)$$

$$i = 0, 1, \dots, k-1.$$

That is, the effective ionization energy is defined as

$$I_i^{\text{eff}} = I_i^{\text{id}} - \Delta I_i, \quad i = 0, 1, \dots, k-1, \quad (7)$$

with

$$I_i^{\text{id}} = \mu_{i+1}^{\text{id}} + \mu_e^{\text{id}} - \mu_i^{\text{id}}, \quad \Delta I_i = \Delta \mu_i - \Delta \mu_{i+1} - \Delta \mu_e, \quad (8)$$

$$i = 0, 1, \dots, k-1.$$

Clearly, I_i^{id} and μ_i^{id} are the ideal ionization potential and chemical potential of Arⁱ⁺. ΔI_i and $\Delta \mu_i$ are the lowering

of ionization potential and the change of chemical potential arising from the interactions. On the other hand, the following Saha equation can be derived from the mass action laws:

$$\frac{n_{i+1}}{n_i} = \frac{U_{i+1}}{U_i} \exp(-\xi - \beta I_i^{\text{eff}}), \quad i = 0, 1, \dots, k-1, \quad (9)$$

where $\beta = 1/(k_B T)$ is the inverse temperature, U_i is the internal partition function of Arⁱ⁺, and $n_i = N_i/V$ and $n_e = N_e/V$ are the number density of Arⁱ⁺ and the electron. $\xi = \frac{\mu_e^{\text{id}}}{k_B T}$ is related to the electron density by

$$F_n(\xi) = \frac{1}{2} n_e \Lambda_e^3, \quad (10)$$

where $\Lambda_e = (2\pi \hbar^2 / m_e k_B T)^{1/2}$ is the thermal de Broglie wavelength of the electron, and

$$F_n(\xi) = \frac{1}{\Gamma(n+1)} \int_0^\infty \frac{x^n dx}{\exp(x-\xi) + 1} \quad (11)$$

is the Fermi integral. $\Gamma(n)$ is the Gamma function with $\Gamma(n+1) = n\Gamma(n)$ and $\Gamma(1/2) = \sqrt{\pi}$.

Equation (9), together with the conversation of mass

$$\sum_{i=0}^k n_i = n_H, \quad (12)$$

and the conversation of charge,

$$n_e = \sum_{i=0}^k i n_i, \quad (13)$$

form a set of close equations, from which the compositions of plasma can be determined if the LIPs are known. $n_H = \frac{\rho}{A} N_A$ denotes the number density of heavy particles, ρ is the mass density, A the atomic weight, and N_A the Avogadro constant.

In fact, the LIPs are not independent of the compositions of the system. It means that the Helmholtz free energy, the LIPs, and the compositions must be self-consistently calculated with appropriate iterative technique. In our SFVT, such a self-consistent calculation is achieved as

Step 1: Guess a value for ξ and set $\Delta I_i = 0$;

Step 2: Calculate $\{n_0, n_1, \dots, n_k, n_e\}$ by solving Eq. (9) under constraints of Eqs. (12) and (13);

Step 3: Calculate a new ξ using Eq. (10) from the obtained compositions;

Step 4: Recalculate $\{n_1, n_2, \dots, n_k, n_e\}$ with the new ξ until the relative error between the new ξ and the old one is less than 10^{-5} ;

Step 5: Calculate the Helmholtz free energy with appropriate model. Then calculate the chemical potentials with Eq. (5), the LIPs with (8), and the effective ionization potentials with (7);

Step 6: Recalculate the compositions with new effective ionization potentials by repeating steps 2–4;

Step 7: Repeat steps 5 and 6, until the difference between new LIPs and the old ones is less than 10^{-3} eV.

Now, let us focus on the free energy model used in our SFVT. The ideal part of free energy is given by the Maxwell-Boltzmann statistics for heavy particles and by the

Fermi integral for electrons,

$$F^{\text{id}} = \sum_{i=0}^k F_i^{\text{id}} + F_e^{\text{id}} = k_B T \sum_{i=0}^k N_i [\ln(n_i \Lambda_i^3) - 1] - k_B T \sum_{i=0}^k N_i \ln U_i^{\text{int}} + N_e k_B T \times \left[\xi - \frac{2}{3} F_{3/2}(\xi) / F_{1/2}(\xi) \right]. \quad (14)$$

The first and the second term are the transitional free energy and the internal free energy of heavy particles, with

$$U_i^{\text{int}} = U_i \exp(-\varepsilon_{i0}/k_B T), \quad (15)$$

where $U_i = \sum_j g_{ij} \exp(-\varepsilon_{ij}/k_B T)$ is the internal partition functions of Ar^{i+} , g_{ij} , and ε_{ij} are the multiplicity and energy of the excited state j of Ar^{i+} . The last term in Eq. (14) is the ideal free energy of electrons and the Fermi integral has been defined by Eq. (11).

It should be mentioned that the influence of interactions on the internal partition functions of atoms and ions has been neglected in Eq. (15). In principle, the exact internal partition functions of atoms and ions in dense plasma should be calculated from the energies of bound electronic states that can be derived by solving the corresponding Schrödinger equations. However, such a calculation is formidable and thus some approximations have to be adopted. A simple treatment of this issue is to use the Planck-Larkin formalism, which was derived from the high-temperature expansion of the Coulomb interactions [41]. The Planck-Larkin formalism has a nice convergence for internal partition function calculation, but the level occupations from it fail to reproduce the experimental data of emissivity [42]. This flaw was also noted by Saumon *et al.* [20]. In our calculations, the internal partition functions of the argon atom and ions, as given by Eq. (15), are simply calculated by weighted summing of the lowest 45 energy levels of them, which are available on the NIST website [43].

The second term of Eq. (4) represents the correction part of the Helmholtz free energy emerged from the interactions among particles, which can be further divided into three parts,

$$F^{\text{cor}} = F^{\text{conf}} + F^{\text{coul}} + F^{\text{pol}}, \quad (16)$$

where F^{conf} is the configuration free energy arising from the interactions between neutral atoms, F^{coul} comes from the interactions between charged particles (including ions and electrons), and F^{pol} stands for the polarization of neutral atoms by ions and electrons.

We treat the interaction among neutral atoms using the fluid perturbation theory and short range repulsion among atoms using a mixture of hard spheres as reference system, that is

$$F^{\text{conf}} = F^{\text{hs}} + F^{\text{pert}}, \quad (17)$$

where F^{hs} is the so-called excess free energy of the mixture of hard spheres. Following the work of Mansoori *et al.* [44], it

is calculated as

$$F^{\text{hs}} = N_H k_B T \left[\frac{3}{2} (1 + y_1 - y_2 - y_3) + \frac{3y_2 + 2y_3}{1 - \eta} + \frac{3}{2} \frac{1 - y_1 - y_2 - y_3/3}{(1 - \eta)^2} + (y_3 - 1) \ln(1 - \eta) \right], \quad (18)$$

with

$$y_1 = \sum_{j>i=0}^k \Delta_{ij} \frac{(d_i + d_j)}{(d_i d_j)^{1/2}},$$

$$y_2 = \sum_{j>i=0}^k \left[\Delta_{ij} \sum_{m=0}^k \left(\frac{\eta_i}{\eta} \right) \frac{\sqrt{d_i d_j}}{d_m} \right],$$

$$y_3 = \left[\sum_i^k \left(\frac{\eta_i}{\eta} \right)^{2/3} \alpha_i^{1/3} \right]^3,$$

$$\Delta_{ij} = \left[\frac{(\eta_i \eta_j)^{1/2}}{\eta} \right] \left[\frac{(d_i - d_j)^2}{d_i d_j} \right] (\alpha_i \alpha_j)^{1/2},$$

$$\eta = \sum_{i=0}^k \eta_i, \quad \alpha_i = \frac{n_i}{n_H}, \quad \eta_i = \frac{1}{6} \pi n_i d_i^3, \quad i = 0, 1, \dots, k,$$

where d_i is the diameter of Ar^{i+} determined by minimization of F^{conf} . The second term in Eq. (17) is a perturbation on the hard sphere system caused by the long range interaction among atoms. It is calculated as

$$F^{\text{pert}} = 2\pi N_0 n_0 \int_{d_0}^{\infty} \phi(r) g_{\text{hs}}(r) r^2 dr, \quad (19)$$

where $\phi(r)$ is the interaction potential between argon atoms. The required radial distribution function $g_{\text{hs}}(r)$ is approximated by that of a reference hard sphere system, as given by Throop *et al.* [45]. The *ab initio* potential function suggested by Nasarbad *et al.* [46] is used to describe the Ar-Ar interaction. The famous exponential-6 (EXP-6) potential function [47] is also used, in order to examine the influence of the potential function on the EOSs.

The contribution of the Coulomb interaction among charged particles, the second term of Eq. (16), is calculated following the work of Stolzmann *et al.* [24],

$$F^{\text{coul}} = F_{ee}^x + F_{ee}^c + F_{ii}^c + F_{ie}^c, \quad (20)$$

where the first two terms are the contributions from the exchange and correlation of electrons, the third one comes from the correlation of ions, and the last one stands for the coupling between electrons and ions. Detailed calculations of these terms can be found in Ref. [24].

The polarization part of free energy, the third term of Eq. (16), is calculated by the second virial coefficients,

$$F^{\text{pol}} = 2k_B T n_0 \sum_i (N_i B_{0,i}), \quad (21)$$

where

$$B_{0,i} = 2\pi \int_{d_0}^{\infty} r^2 (1 - e^{-\beta \phi_{\text{pol}}^i(r)}) dr \quad (22)$$

are the second virial coefficients, and the polarization potential energy is given by

$$\phi_{\text{pol}}^i(r) = -\frac{e^2}{8\pi\epsilon_0} \frac{Z_i\alpha_p}{(r^2 + d_0^2)^2} \left(1 + \frac{r}{r_D}\right)^2 e^{-2r/r_D}, \quad (23)$$

$$i = 1, \dots, k, e,$$

where α_p is the dipole polarizability of the argon atom. d_0 is the diameter of the argon atom determined by the minimization of the configuration free energy. r_D denotes the Debye screening length, defined as

$$r_D = \sqrt{\frac{k_B T \epsilon_0}{e^2 \sum_i Z_i^2 n_i}}. \quad (24)$$

Thus the compositions and the Helmholtz free energies can be self-consistently calculated for the system at a given density and temperature. Based on the obtained compositions and the free energies, the EOSs, and transport properties including electrical conductivity, thermal conductivity, and thermopower can be further calculated. The EOSs are calculated from the total free energy using the following standard thermodynamics relations:

$$P = -\left(\frac{\partial F^{\text{tot}}}{\partial V}\right)_{T, \{N_i\}}, \quad E = -T^2 \left[\frac{\partial(F^{\text{tot}}/T)}{\partial T}\right]_{V, \{N_i\}}, \quad (25)$$

$$S = -\left(\frac{\partial F^{\text{tot}}}{\partial T}\right)_{V, \{N_i\}},$$

where P is the pressure, E the total internal energy, and S the entropy at a given density and temperature. The Hugoniot is determined by fulfilling the Rankine-Hugoniot relation

$$E_H = E_0 + \frac{1}{2}(P_H + P_0)(V_0 - V_H), \quad (26)$$

where P_0, E_0, V_0 are the pressure, internal energy, and the volume of initial state, while P_H, E_H, V_H are those of the final state. Transport properties of such multicomponents plasma are further calculated within the frame of linear response theory.

III. LINEAR RESPONSE THEORY

The linear response theory used here was developed by Röpke, Höhne, Reinholz, Redmer and their colleagues [34–40]. It is an extended version originally derived by Zubarev [48] and can be taken as a general approach to transport properties. Many calculations have manifested that the LRT can be used in a wide range of density and temperature, from the weakly coupled plasma to the strongly coupled one. At the low-density limit, LRT reaches the famous Spitzer formula [49] while for strongly coupled and degenerate systems it accords well with the Ziman theory [50]. Details of LRT can be found in Refs [37,38,40]. Here we only give a brief outline.

In linear response theory, the electrical conductivity σ , the thermopower κ , and the thermal conductivity χ are connected

to the Onsager coefficients by

$$\sigma = e^2 L_{11}, \quad \kappa = \frac{1}{eT} \frac{L_{12}}{L_{11}}, \quad \chi = \frac{1}{T} \left(L_{22} - \frac{L_{12}L_{21}}{L_{11}} \right). \quad (27)$$

The Onsager coefficients are given in the determinant representation (two momentum approximation) as

$$L_{ij} = -\frac{(-h)^{i+j-2}}{V|D|} \begin{vmatrix} 0 & \frac{i-1}{\beta h} \bar{N}_1 - \bar{N}_0 \\ \frac{i-1}{\beta h} N_1 - N_0 & D \end{vmatrix}, \quad (28)$$

with

$$N_i = \begin{pmatrix} N_{i0} \\ N_{i1} \\ N_{i2} \end{pmatrix}, \quad \bar{N}_i = (N_{0i} \quad N_{1i} \quad N_{2i}), \quad (29)$$

$$D = \begin{pmatrix} d_{00} & d_{01} & d_{02} \\ d_{10} & d_{11} & d_{12} \\ d_{20} & d_{21} & d_{22} \end{pmatrix},$$

where $h = 5k_B T/2$ is the enthalpy per particle and V is the normalization volume of system. The elements of the vector N_i and \bar{N}_i represent the generalized particle numbers, i.e., the Kubo products; they are calculated as

$$N_{nm} = N_e \frac{\Gamma(n+m+5/2)}{\Gamma(5/2)} \frac{F_{n+m+1/2}(\beta\mu_e^{\text{id}})}{F_{1/2}(\beta\mu_e^{\text{id}})}. \quad (30)$$

The elements in the D determinant are the equilibrium force-force correlation functions; they are written as a sum of three parts:

$$d_{ij} = d_{ij}^{ea} + d_{ij}^{ei} + d_{ij}^{ee}, \quad (31)$$

and

$$d_{nm}^{ea} = \frac{4Vn_e n_a}{3\beta} \sqrt{\frac{2m_e}{\pi\beta}} \int_0^\infty x^{n+m+2} e^{-x} Q_T^{ea}(x) dx, \quad (32)$$

$$d_{nm}^{ei} = \frac{4Vn_e}{3\beta} \sqrt{\frac{2m_e}{\pi\beta}} \int_0^\infty x^{n+m+2} e^{-x} \left[\sum_j \sqrt{n_j} Q_T^{ej}(x) \right]^2 dx, \quad (33)$$

$$d_{nm}^{ee} = \frac{4}{3} \sqrt{\frac{2m_e}{\pi\beta}} n_e N_e \int_0^\infty x^3 R_{nm}(x) Q_T^{ee}(x) e^{-x} dx, \quad (34)$$

where $R_{n0}(x) = R_{0n}(x) = 0$; $R_{11}(x) = 1$; $R_{21}(x) = R_{12}(x) = 7/2 + x^2$; $R_{22}(x) = 77/4 + 7x^2 + x^4$; $x = \beta E_k$. E_k is the collision energy. Q_T^{ea} , Q_T^{ei} , and Q_T^{ee} are the momentum transfer cross sections of electron scattering by atoms, ions, and other electrons. Following the work of Adams *et al.* [40], we use the first-order Born approximation to calculate Q_T^{ea} , and the T matrix (phase shift) for Q_T^{ei} and Q_T^{ee} . The electron-atom interaction is described by Eq. (23). The electron-ion and electron-electron interactions are described by the Debye-Hückel potential:

$$V^{e-j}(r) = -\frac{e^2 Z_j}{4\pi\epsilon_0 r} e^{-r/r_D}, \quad j = 1, \dots, k, e. \quad (35)$$

It should be mentioned that the contributions arising from the flow of atoms and ions have been neglected since they are much heavier than electrons.

IV. RESULTS AND DISCUSSION

Using the above method, we calculate the compositions, the equations of state, and the transport properties including electron conductivity, thermopower, and thermal conductivity for argon plasma in a wide range of temperature (5–100 kK) and density (10^{-3} – 20 g/cm^3). We firstly focus on the equation of state since it can be directly compared with experimental data, which is necessary to validate our calculations.

A. Equation of state

Figure 1 shows the predicted Hugoniot of liquid argon together with available experimental data for comparison. The Hugoniot calculated using both the *ab initio* [46] and EXP-6 potential [47] are in excellent agreement with shock experiments [51–53] at density below 2.5 g/cm^3 . The interaction between argon atoms is very weak in this region, which makes argon behave like ideal plasma. When the density increases, the interactions become important and a visible dependence of EOS on the potential function is expected. The pressures calculated with the EXP-6 potential are slightly lower than that with *ab initio* potential at density above 2.5 g/cm^3 . Both of them are in good agreement with experimental data.

Figure 2 shows the shock temperature along the Hugoniot together with the degree of ionization. The degree of ionization $Z_{av} = n_e/n_H$ is defined as the ratio of number density of electrons to that of heavy particles. It can be seen that the ionization of argon starts at about 3 g/cm^3 under shock compression. The ionization adsorbs the energy produced by compression and holds down the increase of temperature in the density range of 3 – 4.5 g/cm^3 . The shock temperature calculated with the *ab initio* potential is higher than that with the EXP-6 potential at density above 2.5 g/cm^3 . It is reasonable since the pressure derived from the former is higher than the latter. The difference of temperature caused by potential function is relatively small in the density range that can be reached in experiments ($<4 \text{ g/cm}^3$ for shock liquid argon). It is, however, very large at higher density. For example, above 5.5 g/cm^3 , the temperatures calculated with the *ab initio*

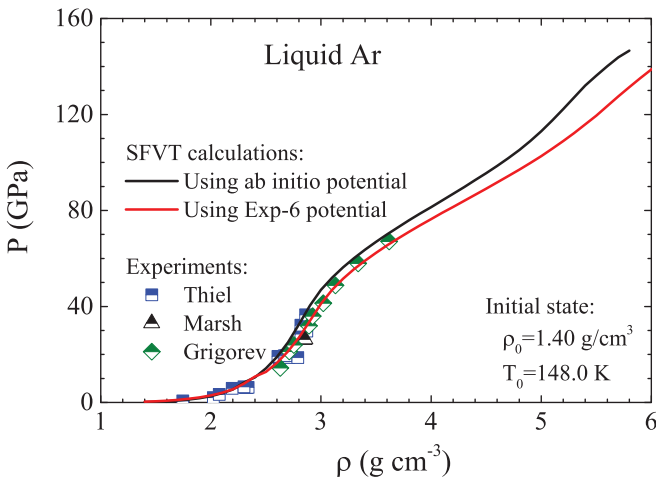


FIG. 1. (Color online) Hugoniot of liquid argon as predicted by SFVT using *ab initio* and EXP-6 potential. The experimental data are taken from Refs. [51–53].

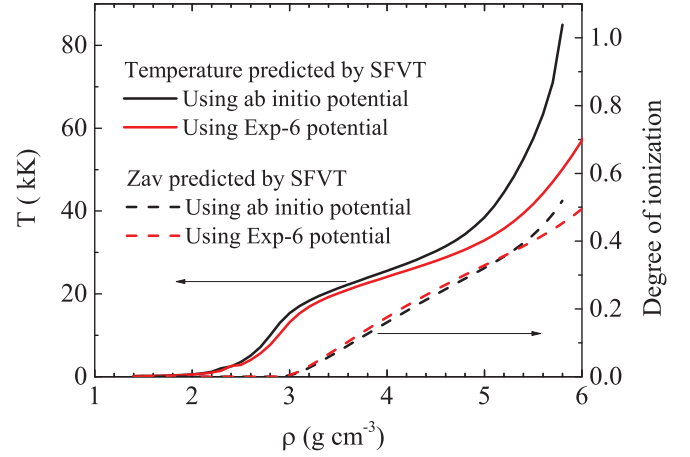


FIG. 2. (Color online) Shock temperature and degree of ionization of liquid argon along the Hugoniot from the same initial state as in Fig. 1.

potential are higher than those with the EXP-6 potential about 10 kK. The pressure given by the EXP-6 potential is closer to experimental data than the *ab initio* potential, but this does not mean that the EXP-6 potential is more appropriate than the *ab initio* potential at higher density which may be out of the range that the EXP-6 potential can describe. More ingenious experiments should be performed to probe the exact EOS at higher density and to test the accuracy of the potentials. We expect that SFVT, as a theoretical model, has a capability of predicting the properties of matter. So, in all the following calculations we select the *ab initio* potential to describe the Ar-Ar interaction because the EXP-6 potential is experiment dependent. In fact, the Hugoniot predicted with this *ab initio* potential is also in good agreement with experimental measurements.

Figure 3 shows the pressure isotherms over a wide range of density and temperature. At density below 1 g/cm^3 , the system

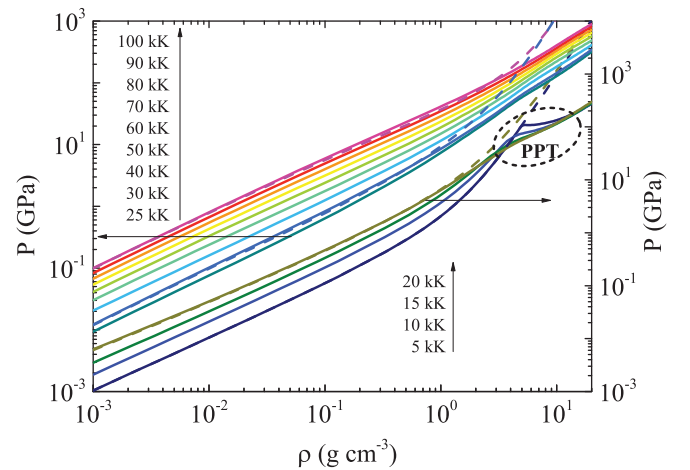


FIG. 3. (Color online) Isotherms of pressure for argon plasma at different temperatures. Solid lines: considering the lowering of ionization potential. Dashed lines: without the lowering of ionization potential for 5, 20, 30, and 100 kK, as representatives. Please note that the pressure scale for the lowest four temperatures (right scale) is different from that for higher temperatures (left scale) for clarity.

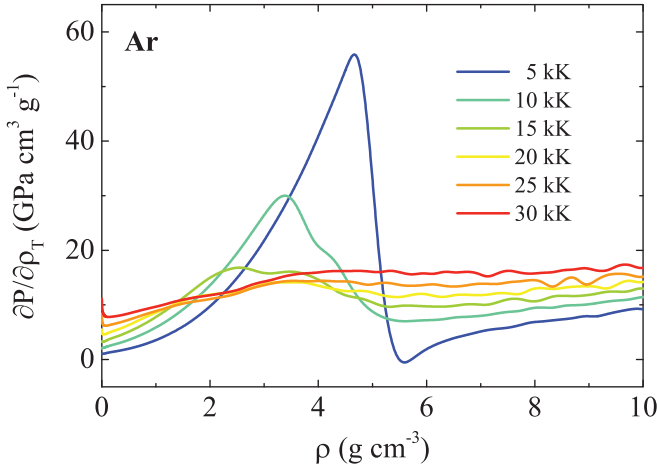


FIG. 4. (Color online) Derivatives of pressure with respect to density are shown as a function of density at different temperatures. It drops at about 5 g/cm^3 as an indication of the plasma phase transition.

behaves like ideal plasma and the pressures with and without considering the LIPs are almost identical. As density increases above 1 g/cm^3 , the pressure considering the LIPs begins to be lower than that without the LIPs, and the higher the density the bigger the difference is.

Figure 3 also shows that when the LIPs are considered, a phase transition occurs at high density and low temperature. To locate the temperature and the density of this phase transition we differentiate the pressure with respect to density $\partial P/\partial \rho$, and the results are shown in Fig. 4. At 5 kK, $\partial P/\partial \rho$ abruptly

drops in $4.5\text{--}5.5 \text{ g/cm}^3$. The drop extends to lower density as temperature increases and finally wears off at 30 kK. It indicates that this phase transition occurs at a temperature below 30 kK and in a density range of $2\text{--}6 \text{ g/cm}^3$ for argon plasma. A similar phase transition, i.e., the so-called plasma phase transition (PPT), was also observed for dense hydrogen [54]. This PPT, however, does not occur in the case of calculation without considering the LIPs which arise from the interactions between particles. That is to say, the PPT is essentially related to the nonideal effects of the system.

B. Compositions

Figure 5 shows the variation of fraction of the electron, Ar, Ar^{+1} , and Ar^{+2} with temperature and density. For a given density, the degree of ionization [Fig. 5(a)] always increases with temperature. For a given temperature, it decreases firstly and then increases with the density, accompanied by the corresponding variation of argon atom fraction [Fig. 5(b)]. This trend indicates that there is a minimum of the degree of ionization along each isotherm. These minima can be regarded as the onset of pressure induced ionization. Its dependence on the temperature is shown in Fig. 5(a) by the thick black line, and the corresponding densities of these minima are also summarized in Table. I. Below 30 kK, the onset density of pressure induced ionization depends weakly on the temperature, but for the higher temperature it increases quickly from 0.53 g/cm^3 at 30 kK to 5.7 g/cm^3 at 100 kK.

The argon plasma mainly consists of Ar and Ar^{+} at temperatures below 40 kK. The fraction of Ar^{+} increases with temperature while that of Ar decreases [Fig. 5(c)]. At temperatures

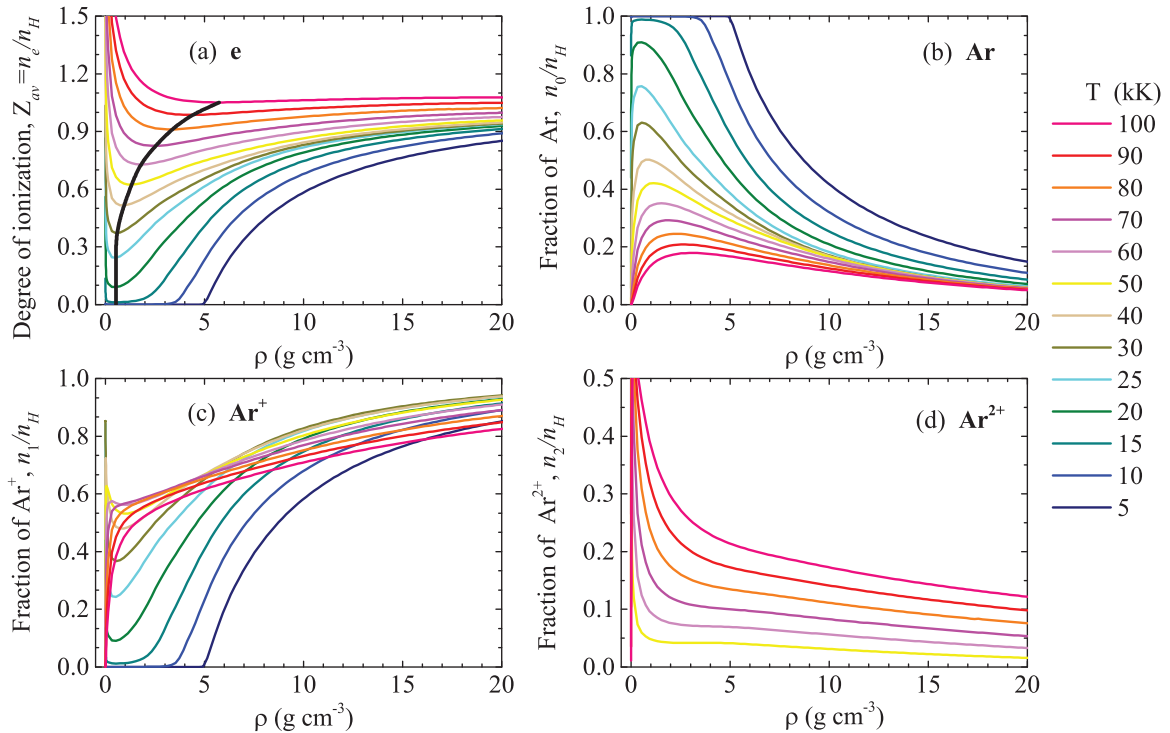


FIG. 5. (Color online) Compositions of argon plasma versus density at different temperatures. (a) Fraction of electron, (b) fraction of Ar, (c) fraction of Ar^{+1} , and (d) fraction of Ar^{+2} . The thick black line in panel (a) is a link of all the minima of degree of ionization, indicating the onset of pressure ionization.

TABLE I. The onset density of pressure induced ionization and the corresponding degree of ionization (n_e/n_H) at varying temperatures.

T (10 ⁴ K)	ρ (g/cm ³)	Degree of ionization
0.5	0.53	1.76×10^{-8}
1.0	0.53	2.79×10^{-4}
1.5	0.53	0.012 20
2.0	0.53	0.091 18
2.5	0.53	0.243 51
3.0	0.53	0.371 41
4.0	0.93	0.515 87
5.0	1.33	0.624 79
6.0	1.73	0.729 21
7.0	2.53	0.825 67
8.0	3.33	0.911 39
9.0	4.33	0.986 40
10.0	5.73	1.051 36

above 40 kK, the fraction of Ar⁺ decreases with temperature due to the second ionization; Ar²⁺ appears in the system at high temperature and its fraction increases with temperature and decreases with density [Fig. 5(d)]. The fractions of ions at higher charge state are not presented because in the range of density and temperature considered here they are only important at very low density where the system behaves like ideal plasma.

It should be noted that the neutral Ar atom never disappears in the whole range of density and temperature considered. It means that the argon plasma is always at partial ionization state; the full ionization state is not reached in this density and temperature region. This observation is different from the results given by COMPTRA04 which has been widely used to derive the transport properties of warm dense matter including hydrogen [54], noble gases [40], and metal plasma [39].

In Fig. 6, the obtained compositions are compared with those by COMPTRA04. It can be seen that the compositions derived with SFVT are in good agreement with COMPTRA04 [55,56] when density is lower than 1 g/cm³, but they are very different at high density. At 10 kK and when density is higher than 3 g/cm³, the degree of ionization given by SFVT is higher than that by COMPTRA04, and both are partially ionized. However, at 15, 20, and 25 kK, COMPTRA04 gives a fully ionized state as the density is higher than a certain value, about 5 – 7 g/cm³. Comparatively, only a partial ionized state is obtained from SFVT.

These divergences between SFVT and COMPTRA04 are rooted in the differences in their free energy model. First, the interaction between neutral atoms is taken into consideration in our SFVT, while in COMPTRA04 it is not. Second, the effect of exciting states on the internal partition functions of atom and ion is included in our SFVT model, while in COMPTRA04 only the ground state is used. Third, the free energy model for charged subsystem used in COMPTRA04 is simpler than that in our SFVT. Additionally, the Hugoniot predicted by SFVT are in good agreement with the experimental

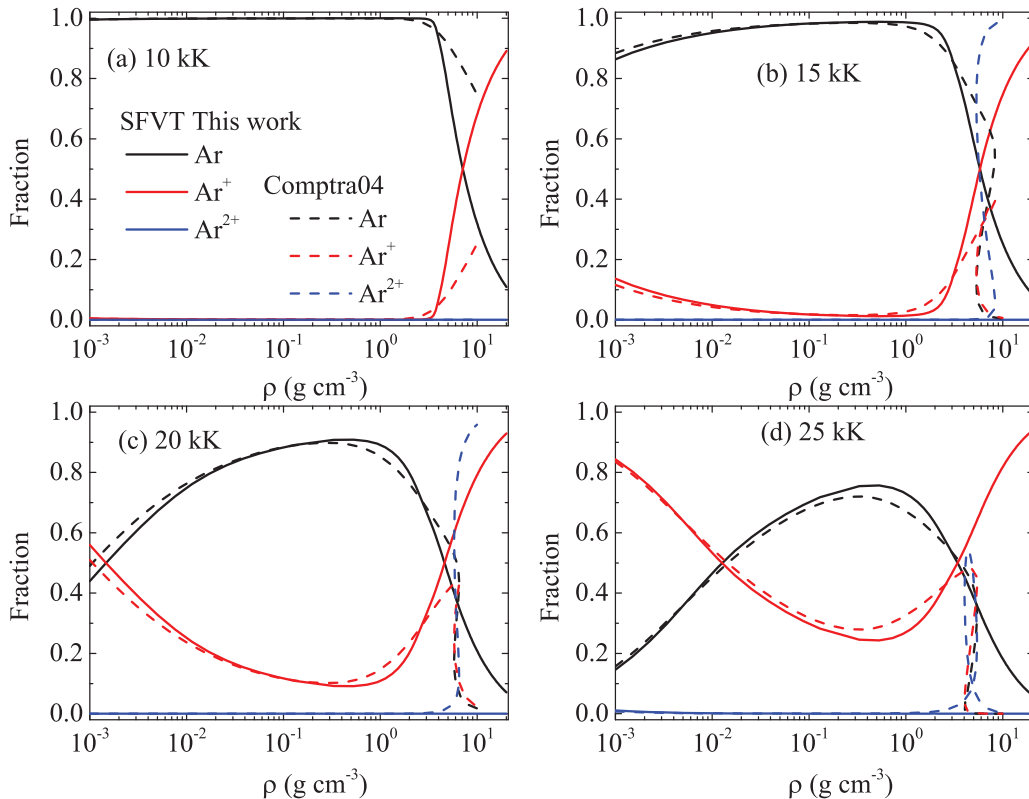


FIG. 6. (Color online) Compositions of argon plasma given by SFVT are compared with those given by COMPTRA04 at four different temperatures. The data of COMPTRA04 are taken from the website [56].

results, while the EOS of argon has not been reported by COMPTRA04.

C. Transport properties

Based on the obtained compositions, the transport properties of argon plasma are then calculated with linear response theory. Figure 7 shows the electrical conductivities as a function of density for typical temperatures. At temperatures below 30 kK, the electrical conductivity decreases at densities below 2 g/cm³, since in this region the degree of ionization decreases with density as a result of the mass action laws. At densities above 3 g/cm³, the electrical conductivity quickly increases with density due to the pressure induced ionization. At temperatures above 40 kK, the electrical conductivity always rises along the density but the dependence on the density becomes weak as temperature increases.

The measured electrical conductivities in shock experiments [57–59] and those calculated by COMPTRA04 [55] are also presented in Fig. 7 for comparison. At densities below 0.3 g/cm³, the electrical conductivities given by COMPTRA04 are in good agreement with ours. From 0.3 g/cm³ to 3 g/cm³, the electrical conductivities given by COMPTRA04 are somewhat higher. For higher density they are lower than ours. These divergences arise from the differences in compositions. As has been discussed, the compositions given by COMPTRA04 are very different from those by SFVT because the interaction among neutral argon atoms and the effect of exciting states were neglected in the free energy model of COMPTRA04. In fact, the electrical conductivities given by both COMPTRA04 and SFVT are in good agreement with experimental results, and SFVT seems to be closer to the values of experiments than COMPTRA04.

Another interesting observation is that the calculated electrical conductivity isotherms intercross with each other at density about 6 g/cm³. That is, as the density increases, the dependence of the electrical conductivity on the temperature is inverted at a certain density, which can be taken as an indication of the nonmetal-metal transition (NMMT) [60,61]. At densities below the transition the electrical conductivity increases with temperature due to thermal ionization. At densities above the transition the electrical conductivity

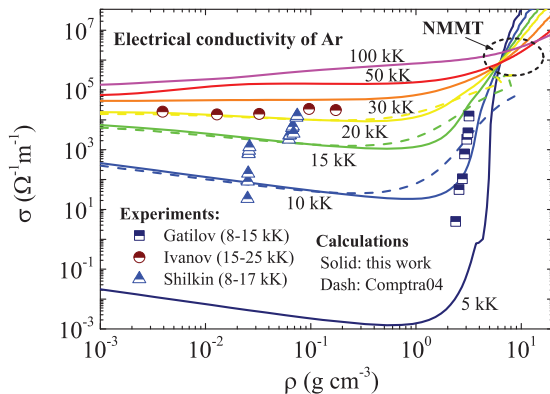


FIG. 7. (Color online) Isotherms of electrical conductivity at different temperatures. Solid lines: SFVT+LRT. Dashed lines: Results of COMPTRA04 [56] at three temperatures. Symbols: data of gas gun and explosive experiments [57–59].

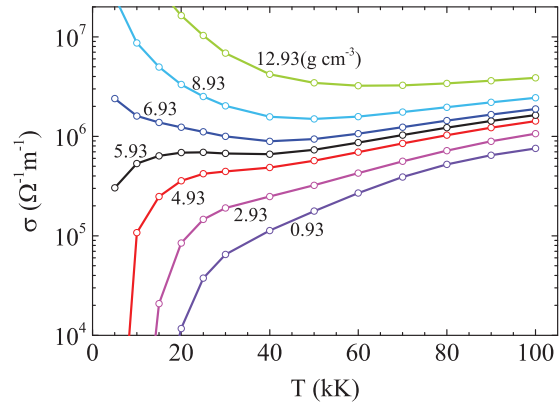


FIG. 8. (Color online) Electrical conductivity versus temperature at different densities for argon plasma.

decreases with temperature, which is a typical characteristic of metal. This behavior is also illustrated in Fig. 8, which shows the electrical conductivity as a function of temperature for different densities near the NMMT. When density is lower than 5 g/cm³, the conductivity rises along the whole temperature range considered due to thermal ionization. When the density is higher than 5.9 g/cm³, the conductivity decreases with temperatures below 40 kK, and then slightly increases with temperature for higher temperatures. The decrease of conductivity with temperature is a characteristic of the metallic phase. It can be found that the minimum density of the metallization of argon plasma is about 5.8 g/cm³, presenting at about 30–40 kK.

Figure 9 shows the calculated thermal conductivities together with those given by COMPTRA04 [56]. The thermal conductivity is very small at low density and low temperature; it increases with temperature and decreases with density in this region. At high density, the thermal conductivity quickly increases with density and decreases with temperature. These trends are similar to electrical conductivity due to the fact that the thermal conductivity presented here arises from the flow of electrons; the contributions of ions and atoms have been neglected in our calculations.

The variations of thermopower with density and temperature are shown in Fig. 10(a) and are compared with the

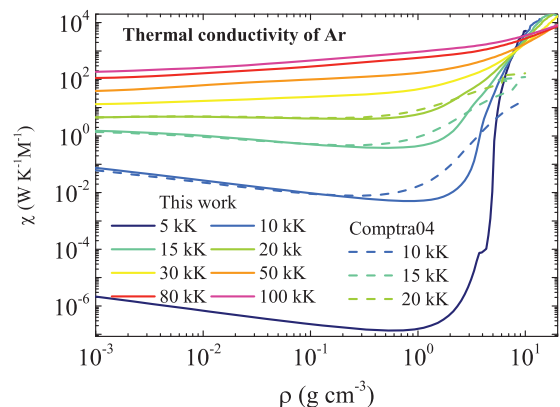


FIG. 9. (Color online) Thermal conductivity versus density at different temperatures for argon plasma together with those given by COMPTRA04 [56].

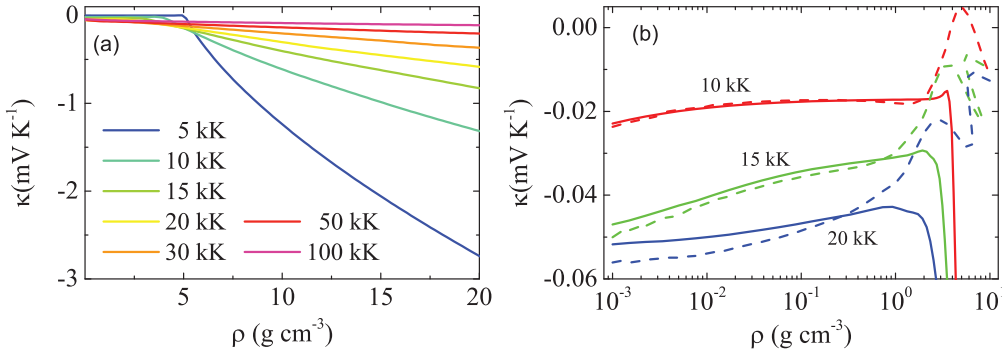


FIG. 10. (Color online) Thermopower versus density at different temperatures for argon plasma. (a) Results of this work (SFVT+LRT); (b) comparison with COMPTRA04 [56].

results of COMPTRA04 [56] in Fig. 10(b). At density below 2 g/cm^3 , the thermopower of argon decreases with density and increases with temperature, but the dependence on the density and temperature is very weak, while at density above 2 g/cm^3 , the thermopower increases quickly with density and decreases with temperature. The influence of density on thermopower is weakened as temperature increases. At high density, thermopower predicted by COMPTRA04 decreases with density and even becomes positive at some density, while the thermopower predicted by our SFVT is always negative and its variation with density is more regular.

D. Effects of many-particle correlations and dynamic screening

It should be noticed that the Debye-Hückel potential, Eq. (35), from which the required momentum transfer cross sections are derived, is only accurate for low-density plasma where the pair-particle correlations are dominant. As the density increases, the effects of higher-order many-particle correlations should be considered. In Ref. [62], an integrodifferential equation for the effective interaction considering the many-particle correlations was obtained based on the solution of the Bogolyubov equations for the nonideal plasma, and an analytic effective pair potential that accounts for the three-particle correlation effects was also given with the spline approximation,

$$V^{e-j}(r) = -\frac{Z_j e^2}{4\pi\epsilon_0 r} \exp(-r/r_D) \frac{1 + \gamma f(r)/2}{1 + c(\gamma)}, \quad (36)$$

$$j = 1, \dots, k, e,$$

where $\gamma = e^2/r_D k_B T$ is a nonideal parameter of plasma, $f(r) = (e^{-\sqrt{\gamma}r/r_D} - 1)(1 - e^{-2r/r_D})/5$, and $c(\gamma) \cong -0.008617 + 0.455861\gamma - 0.108389\gamma^2 + 0.009377\gamma^3$. This effective potential has been used to study the Coulomb Bremsstrahlung process [63] and the electron captures [64]. Here it is used to illustrate the influence of higher-order many-particle correlations on the transport properties.

The calculated electrical conductivities using the momentum transfer cross sections derived with Eq. (36) are compared with those using Eq. (35) in Fig. 11. At low density and low temperature, the effect of many-particle correlations on the electrical conductivity is very slight. However, as the temperature increases, especially at high density, the effect of many-particle correlations becomes obvious. At relatively

low density, it leads to the increase of electrical conductivity, while at very high density it results in the decrease of electrical conductivity.

Another shortcoming of Eqs. (23) and (35) is that the dynamic screening is not taken into consideration. For a particle moving at a speed less than the average thermal velocity, the static screening approximation is still acceptable. In the opposite case of high-speed collisions, the dynamic screening effects are expected to be significant. The dynamic screening can be introduced with the following velocity-dependent screening potential [65]:

$$V^{e-j}(r) = -\frac{Z_j e^2}{4\pi\epsilon_0 r} \exp[-r/r_0(v)], \quad (37)$$

where $r_0(v) = r_D(1 + v/v_{th})^{1/2}$, $v_{th} = \sqrt{k_B T/m_e}$ is the averaged thermal velocity of electrons, and v the relative velocity of collision pairs. Clearly, the static Debye-Hückel potential is reached as the collision velocity $v \rightarrow 0$. This is a phenomenological and simple approach to trace the dynamic screening, but it grasps the essential of dynamic screening and has been used to study the elastic collisions [64]. Similar treatment is also applied to the polarization potential, Eq. (23).

The electrical conductivities calculated based on dynamic screening potentials are compared with those based on static screening potentials in Fig. 12. It can be seen that the dynamic screening results in remarkable decrease of the electrical conductivity because the shielding of the interactions

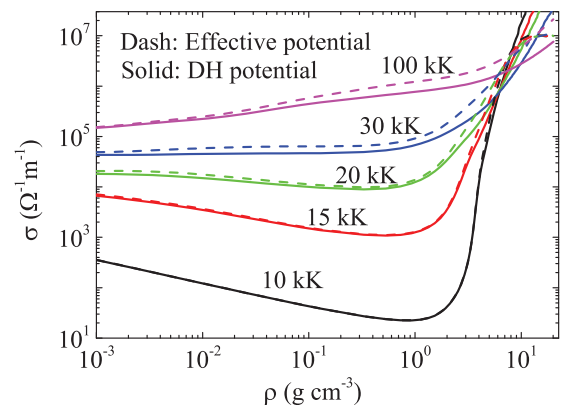


FIG. 11. (Color online) Effects of many-particle correlations on the electrical conductivity of argon.

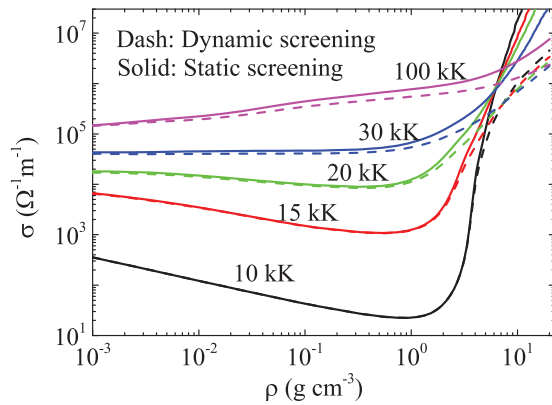


FIG. 12. (Color online) Effects of dynamic screening on the electrical conductivity of argon.

is weakened for the case of high-velocity collisions. The influence of dynamic screening on the transport properties is enhanced as the temperature and density increase.

V. CONCLUSION

Self-consistent fluid variational theory (SFVT) is extended to study argon plasma in a wide range of density ($0.001\text{--}20\text{ g/cm}^3$) and temperature ($5\text{--}100\text{ kK}$). The equations of state predicted by SFVT are found in good agreement with experimental results. The so-called plasma phase transition was observed at low temperature ($<30\text{ kK}$) and at density about $2\text{--}6\text{ g/cm}^3$ for argon. Based on the

compositions given by SFVT, the electrical conductivity, thermal conductivity, and thermopower are calculated for argon with linear response theory. The obtained electrical conductivities are also found in good agreement with available experimental measurements. The nonmetal-metal transition is recognized by the temperature dependence of the electrical conductivity. The minimum density for metalizing argon is found at about 5.8 g/cm^3 , occurring at $30\text{--}40\text{ kK}$. The effects of the many-particle correlations and dynamic screening are studied based on effective potentials. The dynamic screening leads to the decrease of electrical conductivity, while the many-particle correlations increase the electrical conductivity at low density and decrease it at high density. Our calculations illustrate that of the combination of SFVT and LRT is a promising route to understanding the properties of warm dense matter.

ACKNOWLEDGMENTS

This work received financial support from the National Natural Science Foundation of China (Grant No. 11074226), the Science and Technology Development Foundation of China Academy of Engineering Physics (Grants No. 2013A0101001 and No. 2012B0101001), and the Foundation of Laboratory of Shock Wave and Detonation Physics, CAEP (Grant No. 9140C670104120C67247). W.L.Q. expresses thanks for the support from the National Natural Science Foundation of China (Grant No. 51365027) and from the Young Scholars Science Foundation of Lanzhou Jiaotong University (Grant No. 2011027).

-
- [1] M. Koenig, A. Benuzzi-Mounaix, A. Ravasio, T. Vinci, N. Ozaki, S. Lepape, D. Batani, G. Huser, T. Hall, D. Hicks, A. MacKinnon, P. Patel, H. S. Park, T. Boehly, M. Borghesi, S. Kar, and L. Romagnani, *Plasma Phys. Controlled Fusion* **47**, B441 (2005).
 - [2] S. X. Hu, B. Militzer, V. N. Goncharov, and S. Skupsky, *Phys. Rev. Lett.* **104**, 235003 (2010).
 - [3] N. Nettelmann, B. Holst, A. Kietzmann, M. French, and R. Redmer, *Astrophys. J.* **683**, 1217 (2008).
 - [4] M. D. Knudson, M. P. Desjarlais, R. W. Lemke, T. R. Mattsson, M. French, N. Nettelmann, and R. Redmer, *Phys. Rev. Lett.* **108**, 091102 (2012).
 - [5] M. A. Morales, C. Pierleoni, and D. M. Ceperley, *Phys. Rev. E* **81**, 021202 (2010).
 - [6] B. Militzer, *Phys. Rev. B* **79**, 155105 (2009).
 - [7] P. R. Levashov, V. S. Filinov, M. Bonitz, and V. E. Fortov, *J. Phys. A* **39**, 4447 (2006).
 - [8] K. P. Driver and B. Militzer, *Phys. Rev. Lett.* **108**, 115502 (2012).
 - [9] I. Kwon, L. Collins, J. Kress, and N. Troullier, *Phys. Rev. E* **54**, 2844 (1996).
 - [10] P. M. Kowalski, S. Mazevet, D. Saumon, and M. Challacombe, *Phys. Rev. B* **76**, 075112 (2007).
 - [11] K. U. Plagemann, P. Sperling, R. Thiele, M. Desjarlais, C. Fortmann, T. Döppner, H. Lee, S. Glenzer, and R. Redmer, *New J. Phys.* **14**, 055020 (2012).
 - [12] S. Mazevet and G. Zerah, *Phys. Rev. Lett.* **101**, 155001 (2008).
 - [13] T. R. Mattsson and M. P. Desjarlais, *Phys. Rev. Lett.* **97**, 017801 (2006).
 - [14] A. S. Mikhaylushkin, S. I. Simak, L. Dubrovinsky, N. Dubrovinskaia, B. Johansson, and I. A. Abrikosov, *Phys. Rev. Lett.* **99**, 165505 (2007).
 - [15] R. Piron and T. Blenski, *High Energy Density Phys.* **7**, 346 (2011).
 - [16] G. Faussurier, C. Blancard, P. Cossé, and P. Renaudin, *Phys. Plasmas* **17**, 052707 (2010).
 - [17] M. W. C. Dharma-wardana, *Int. J. Quantum Chem.* **112**, 53 (2012).
 - [18] D. Saumon, C. E. Starrett, J. D. Kress, and J. Clerouin, *High Energy Density Phys.* **8**, 150 (2012).
 - [19] M. Ross, F. Rogers, N. Winter, and G. Collins, *Phys. Rev. B* **76**, 020502(R) (2007).
 - [20] D. Saumon and G. Chabrier, *Phys. Rev. A* **44**, 5122 (1991).
 - [21] D. Saumon and G. Chabrier, *Phys. Rev. A* **46**, 2084 (1992).
 - [22] H. C. Graboske, Jr., D. J. Harwood, and F. J. Rogers, *Phys. Rev.* **186**, 210 (1969).
 - [23] W. Stolzmann and T. Blöcker, *Astron. Astrophys.* **361**, 1152 (2000).
 - [24] W. Stolzmann and T. Blöcker, *Astron. Astrophys.* **314**, 1024 (1996).

- [25] C. Winisdoerffer and G. Chabrier, *Phys. Rev. E* **71**, 026402 (2005).
- [26] V. K. Gryaznov, S. V. Ayukov, V. A. Baturin, I. L. Iosilevskiy, A. N. Starostin, and V. E. Fortov, *J. Phys. A: Math. Gen.* **39**, 4459 (2006).
- [27] V. Gryaznov and I. Iosilevskiy, *J. Phys. A: Math. Gen.* **42**, 214007 (2009).
- [28] V. Schwarz, H. Juranek, and R. Redmer, *Phys. Chem. Chem. Phys.* **7**, 1990 (2005).
- [29] Q. F. Chen, L. C. Cai, Y. J. Gu, and Y. Gu, *Phys. Rev. E* **79**, 016409 (2009).
- [30] Q. F. Chen, Y. Zhang, L. C. Cai, Y. J. Gu, and F. Q. Jing, *Phys. Plasmas* **14**, 012703 (2007).
- [31] Q. F. Chen, L. C. Cai, Y. Zhang, and Y. J. Gu, *J. Chem. Phys.* **128**, 104512 (2008).
- [32] Q. F. Chen, J. Zheng, Y. J. Gu, Y. L. Chen, and L. C. Cai, *Phys. Plasmas* **18**, 112704 (2011).
- [33] Q. F. Chen, L. C. Cai, Y. J. Gu, J. Zheng, and G. F. Ji, *Phys. Lett. A* **374**, 3875 (2010).
- [34] G. Röpke and F. E. Höhne, *Phys. Status Solidi B* **107**, 603 (1981).
- [35] F. E. Höhne, R. Redmer, G. Röpke, and H. Wegener, *Phys. A* **128**, 643 (1984).
- [36] H. Reinholz, R. Redmer, and D. Tamme, *Contrib. Plasma Phys.* **29**, 395 (1989).
- [37] H. Reinholz, R. Redmer, and S. Nagel, *Phys. Rev. E* **52**, 5368 (1995).
- [38] R. Redmer, *Phys. Rev. E* **59**, 1073 (1999).
- [39] S. Kuhlbrodt and R. Redmer, *Phys. Rev. E* **62**, 7191 (2000).
- [40] J. R. Adams, H. Reinholz, R. Redmer, V. B. Mintsev, N. S. Shilkin, and V. K. Gryaznov, *Phys. Rev. E* **76**, 036405 (2007).
- [41] W. Däppen, L. Anderson, and D. Mihalas, *Astrophys. J.* **319**, 195 (1987).
- [42] W. L. Wiese, D. E. Kelleher, and N. R. Paquette, *Phys. Rev. A* **6**, 1132 (1972).
- [43] <http://www.nist.gov/pml/data/asd.cfm>
- [44] G. Mansoori, N. Carnahan, K. Starling, and T. Leland, *J. Chem. Phys.* **54**, 1523 (1971).
- [45] G. Throop and R. Bearman, *J. Chem. Phys.* **42**, 2408 (1965).
- [46] A. E. Nasrabad and R. Laghaei, *J. Chem. Phys.* **125**, 084510 (2006).
- [47] M. Ross and B. Alder, *J. Chem. Phys.* **46**, 4203 (1967).
- [48] D. N. Zubarev, *Nonequilibrium Statistical Thermodynamics* (Consultants Bureau, New York, 1974).
- [49] L. Spitzer, Jr. and R. Härm, *Phys. Rev.* **89**, 977 (1953).
- [50] J. M. Ziman, *Philos. Mag.* **6**, 1013 (1961).
- [51] M. van Thiel and B. J. Alder, *J. Chem. Phys.* **44**, 1056 (1966).
- [52] S. P. Marsh, *LASL Shock Hugoniot Data* (University of California Press, Berkeley, 1980).
- [53] F. V. Grigo'rev, O. L. Mikhailova, M. A. Mochalov, and V. D. Urlin, *Zh. Eksp. Teor. Fiz.* **88**, 1271 (1985) in Russian.
- [54] B. Holst, N. Nettelmann, and R. Redmer, *Contrib. Plasma Phys.* **47**, 368 (2007).
- [55] S. Kuhlbrodt, B. Holst, and R. Redmer, *Contrib. Plasma Phys.* **45**, 73 (2005).
- [56] <http://www.statistische.physik.uni-rostock.de/en/compra/>.
- [57] L. A. Gatilov, V. D. Glukhodedov, F. V. Grigor'ev, S. B. Kormer, L. V. Kuleshova, and M. A. Mochalov, *J. Appl. Mech. Tech. Phys.* **26**, 88 (1985).
- [58] Yu. V. Ivanov, V. B. Mintsev, V. E. Fortov, and A. N. Dremin, *Sov. Phys. JETP* **44**, 112 (1976).
- [59] N. S. Shilkin, S. V. Dudin, V. K. Gryaznov, V. B. Mintsev, and V. E. Fortov, *Sov. Phys. JETP* **97**, 922 (2003).
- [60] M. I. Eremets and I. A. Troyan, *Nat. Mater.* **10**, 927 (2011).
- [61] P. P. Edwards and M. J. Sienko, *Int. Rev. Phys. Chem.* **3**, 83 (1983).
- [62] F. B. Baimbetov, K. T. Nurekenov, and T. S. Ramazanov, *Phys. Lett. A* **202**, 211 (1995).
- [63] Y.-D. Jung, *Eur. Phys. J. D* **11**, 291 (2000).
- [64] C. G. Kim and Y.-D. Jung, *Phys. Plasmas* **19**, 014502 (2012).
- [65] D. Kremp, M. Schlanges, and W.-D. Kraeft, *Quantum Statistics of Nonideal Plasmas* (Springer, Berlin, 2005).